

# Modification of single molecule fluorescence close to a nanostructure: radiation pattern, spontaneous emission and quenching

S. Kühn,<sup>\*</sup> G. Mori, M. Agio, and V. Sandoghdar<sup>†</sup>

*Laboratorium für Physikalische Chemie,  
ETH Zürich, 8093 Zürich, Switzerland*

## Abstract

The coupling of nanostructures with emitters opens ways for the realization of man-made subwavelength light emitting elements. In this article, we investigate the modification of fluorescence when an emitter is placed close to a nanostructure. In order to control the wealth of parameters that contribute to this process, we have combined scanning probe technology with single molecule microscopy and spectroscopy. We discuss the enhancement and reduction of molecular excitation and emission rates in the presence of a dielectric or metallic nanoparticle and emphasize the role of plasmon resonances in the latter. Furthermore, we examine the spectral and angular emission characteristics of the molecule-particle system. Our experimental findings are in excellent semi-quantitative agreement with the outcome of theoretical calculations. We express our results in the framework of optical nanoantennae and propose arrangements that could lead to the modification of spontaneous emission by more than 1000 times.

---

<sup>\*</sup>Present address: University of California at Santa Cruz, CA 95067 USA

<sup>†</sup>Electronic address: vahid.sandoghdar@ethz.ch

## I. INTRODUCTION

The radiative properties of an emitter, such as the angular distribution of its emitted power, its spectrum and fluorescence lifetime can be strongly modified in confined geometries. One of the earliest indications of these phenomena was pointed out by A. Sommerfeld who considered the radiation of a dipole close to a surface [1]. Another seminal proposal was made by E. M. Purcell on the enhancement of the decay rate of an atomic excited state inside a cavity [2]. The pioneering experimental work dates back to around 1970 when K. H. Drexhage showed that the fluorescence lifetimes of emitters placed very close to a flat mirror were different from those in free space [3]. In the 1980s and 1990s several groups have demonstrated the possibility of controlling radiative decay rates and the emission pattern by putting emitters in confined geometries such as the spaces between two flat substrates, between the mirrors of high-finesse cavities and in whispering gallery mode resonators [4, 5]. In all these cases the dimensions of the geometries surrounding the emitter have been superior to the transition wavelength of interest. Considering that advances in nanosciences over the past decades have made the understanding and manipulation of the nanometer scale processes both more accessible and desirable, it is highly interesting to investigate the radiative properties of atoms, ions, molecules or quantum dots using subwavelength boundaries. At our laboratories, we have conducted both theoretical [6, 7, 8, 9] and experimental [10, 11, 12, 13] research in this direction. Before we present some of our most recent results, we find it instructive to provide a brief historical overview of some of the relevant activities in the past three decades.

A few years after the work of Drexhage on the change of the fluorescence lifetime, researchers found out experimentally that the Raman scattering signal from molecules can be enhanced close to rough metallic surfaces [14]. Soon after this discovery, it was proposed that an important contribution to the observed effect can come from the enhancement of the electromagnetic fields close to sharp edges of a rough surface [15]. Furthermore, it was pointed out that this lightning rod type of effect can be strengthened if surface plasmon resonances are supported by the system [16, 17]. In order to model the situation at hand, scientists simplified a rough surface by considering single or small aggregates of metallic nanoparticles such as spheres and ellipsoids. It was also pointed out that not only the excitation channel is enhanced due to the strong near fields, but also the emission of a dipole is modified close to a nanoparticle [18, 19, 20], much like the effect observed by Drexhage. Early experimental efforts of the 1970s and 1980s used ensembles of molecules and nanoparticles, but the inherent inhomogeneities in such experiments plagued clear comparisons with the theoretical predictions. The main obstacle is that the radiative properties of an emitter

such as a molecule depend very strongly on its orientation and separation from the nanostructure as well as the shape, material and size of the latter. In addition, the wavelength dependence of the dielectric constants of the nanostructure determines the strength of the modifications at the emission and absorption wavelengths of the emitter.

Advances in nano-optics have brought about various new tools for studying single molecules [21] and single metallic nanoparticles [22, 23, 24, 25] both spatially and spectrally. These developments motivated the investigation of the Raman enhancement at the level of a single molecule and a single nanoparticle [26] or small aggregates [27]. In particular, scanning probe techniques offered a convenient way of controlling the coupling between a molecule and a nanostructure. The first impulse of this method was to modify the fluorescence lifetime of a fluorescent molecule by approaching it to a metallized near-field tip [28, 29]. At about the same time sharp extended tips were introduced as subwavelength sources of field enhancement for obtaining better resolution in near-field microscopy [30, 31, 32]. Later, the same arrangement was successfully applied to subwavelength studies of SERS on single nano-objects such as carbon nanotubes [33]. However, experience has shown that production of well-defined and reproducible tips is a very tedious task [34]. Furthermore, a theoretical treatment of extended tips is nontrivial and could lead to numerical artefacts. To remedy these problems, several years ago we set out to perform experiments where a well characterized metallic nanoparticle is attached to a dielectric tip [35] to act as a local enhancer that can be positioned at will in front of a single molecule [11], as originally proposed by J. Wessel in 1985 in the context of SERS and nonlinear near-field microscopy [36]. As we show in what follows, this strategy has allowed us to control the relative distances and orientations of single molecule and gold nanosphere.

In the past few years, many of the ideas mentioned above have been reformulated in a new framework based on the concepts from antenna theory [37]. Different groups have worked to extend the conventional antenna designs to the nanometer scale [38, 39] although the very different behavior of metals at optical and microwave or radio frequencies makes this extension nontrivial. It turns out that again a single gold nanoparticle that supports plasmon resonances can act as a very simple and elementary antenna. In this article we show that such a subwavelength particle can serve as a receiving and transmitting subwavelength resonant antenna with a dipolar radiation pattern and a well-defined resonance spectrum. The great advantage of this system is that its scattering properties and plasmon spectra are well described analytically using Mie theory [23, 40]. In the last section of this article, we discuss realistic designs for two-particle antennae and how one could reduce the effect of quenching due to losses in metals.

The paper is organized as follows. We will first introduce a simple model of a dipole close to a sphere as the basis for our calculations and the interpretation of the experimental results. In the following section we will present a selection of scanning probe near-field images of single molecules. We will start with a simple glass tip and establish the modification of excitation and emission properties in the absence of material absorption. Then we will focus specifically on the quenching phenomenon by adding a thin layer of chromium onto the tip. The choice of chromium deliberately avoids resonances. We then move on to using a tip that carries a single gold nanoparticle at its apex. This tip produces the strongest effect on the excitation, the decay rate, the emission spectrum and the radiation pattern of a molecule reported to date. To complete these studies we will present design guidelines and experimental results on resonant antenna structures involving two nanoparticles.

## II. THEORETICAL CONCEPTS

In this section, we briefly discuss the influence of a nanostructure on the interaction between an incident laser field and a fluorescent molecule, which we treat as a classical oscillating dipole (see fig. 1). Generally, the fluorescence signal  $S_f$  from the molecule can be expressed as [41]:

$$S_f(\hat{\mathbf{d}}, \mathbf{r}) = c \xi(\hat{\mathbf{d}}, \mathbf{r}) K(\hat{\mathbf{d}}, \mathbf{r}) \eta(\hat{\mathbf{d}}, \mathbf{r}) \quad (1)$$

for the weak excitation regime far from saturation. Here the coefficient  $c = S_0/(\xi_0\eta_0)$  normalizes the signal to the fluorescence  $S_0$  of the unperturbed molecule,  $\xi$  is the collection efficiency which can also depend on the system parameters, and  $K$  is the ratio of the excitation rates in presence and absence of the tip given by

$$K(\hat{\mathbf{d}}, \mathbf{r}) = |\mathbf{d} \cdot \mathbf{E}_{\text{loc}}(\mathbf{r})|^2 / |\mathbf{d} \cdot \mathbf{E}_{\text{inc}}(\mathbf{r})|^2 . \quad (2)$$

Finally,  $\eta$  is the apparent quantum yield, defined as

$$\eta(\hat{\mathbf{d}}, \mathbf{r}) = \frac{\gamma_{\text{rad}}(\hat{\mathbf{d}}, \mathbf{r})}{\gamma_{\text{rad}}(\hat{\mathbf{d}}, \mathbf{r}) + \gamma_{\text{nr}}(\hat{\mathbf{d}}, \mathbf{r})} \quad (3)$$

where  $\gamma_{\text{rad}}$  and  $\gamma_{\text{nr}}$  denote the radiative and nonradiative decay rates of the excited state lifetime. Thus, the key parameters are the field  $\mathbf{E}_{\text{loc}}(\mathbf{r})$  around the tip and the decay rates  $\gamma_{\text{rad}}(\mathbf{d}, \mathbf{r})$  and  $\gamma_{\text{nr}}(\mathbf{d}, \mathbf{r})$  in the presence of the nanostructure.

In the case of a spherical or ellipsoidal particle, the nanostructure can be fully described using generalized Mie theory for different incident fields [42, 43, 44, 45, 46]. Further simplifications

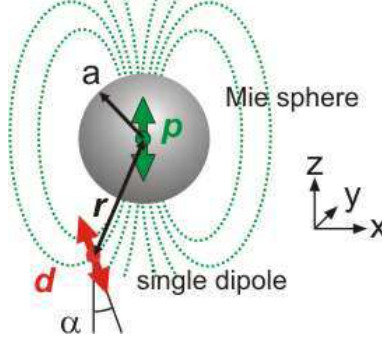


FIG. 1: A nanosphere of radius  $a$  placed close to a dipolar emitter.  $r$  is distance between the sphere center and the emitter, and  $\alpha$  denotes the tilt angle of the emitter's dipole moment.

apply for small spheres if  $ka \ll 1$  where  $k$  is the magnitude of the relevant wavevector and  $a$  is the radius of the sphere. The optical response is then identical to that of a dipole with the moment  $\mathbf{p} = 4\pi\alpha\mathbf{E}_{inc}$  where  $\alpha$  is the electrostatic polarizability of the sphere and  $E_{inc}$  denotes the incident field [42, 47]. The resulting field around the sphere is then given by  $\mathbf{E}_{loc}(\mathbf{r}) = \mathbf{E}_s(\mathbf{p}, \mathbf{r}) + \mathbf{E}_{inc}(\mathbf{r})$  where  $E_s$  is the scattered field due to  $\mathbf{p}$ . Metallic nanoparticles can respond resonantly upon the excitation of surface plasmon-polaritons, which are the optical pendant to the resonances of radio antennae [42]. As we will see below, the interaction of various dielectric and metallic tips can be described to a good degree by approximating them as small spheres.

Using this model in conjunction with eqn. 2 has the following consequences. The magnitude of the excitation enhancement depends on the position  $\mathbf{r}$  and the relative orientations between  $\mathbf{p}$  and the molecular dipole moment  $\mathbf{d}$ . The highest excitation enhancement is expected when  $\hat{\mathbf{r}}$ ,  $\hat{\mathbf{p}}$  and  $\hat{\mathbf{d}}$  are aligned. In the quasi-static dipole approximation, the magnitude of  $K$  then goes as  $1/r^6$  and reaches a finite maximum on the surface (i.e.  $r = a$ ), independent of the size of the sphere. Close to the surface,  $E_s$  will dominate over  $E_{inc}$  provided that there is an appreciable polarization. At distances where the magnitudes of  $E_s$  and  $E_{inc}$  are similar their interference leads to a modulation of  $K$  [48].

The emission of the molecule is also altered in the presence of the sphere [49, 50] via a change in the radiative decay rate  $\gamma_{rad}$  [51, 52, 53, 54] and in the non-radiative rate  $\gamma_{nr}$  if the material of the sphere absorbs light [55]. Without engaging in a detailed discussion, we make the following remarks that can provide a quick intuitive picture of the physics at hand. The presence of a nanoparticle can result in a change of the apparent quantum yield  $\eta$  (eqn. 3) of the joint molecule-sphere system [53, 56, 57].  $\eta$  may be increased for a molecule with a small initial yield  $\eta^0 < 1$  [57] but can only decrease if  $\eta^0 \approx 1$ . Furthermore,  $\gamma_{nr}(\mathbf{d}, \mathbf{r})$  will increase as  $1/(r - a)^6$  when the

molecule approaches the absorbing surface, leading to the notorious fluorescence quenching for  $r \rightarrow a$ . The emission and the excitation processes are linked in accordance with the reciprocity theorem [58, 59]. In other words, an antenna effect in the enhancement of the excitation also leads to the enhancement of the emission rate. Again, maximal radiation is achieved when  $\hat{\mathbf{d}}$  is oriented radially and is parallel to  $\hat{\mathbf{p}}$  [106].  $\mathbf{d}$  and  $\mathbf{p}$  then add up to form a large dipole moment. The opposite is the case if  $\hat{\mathbf{d}}$  lies tangential to the sphere surface. Here the resulting  $\hat{\mathbf{p}}$  becomes antiparallel to  $\hat{\mathbf{d}}$  and their summation is destructive. The magnitude of  $\mathbf{p}$  has a  $1/r^6$  dependence to the lowest (dipole-) approximation. Furthermore, the spectral dependence of  $\epsilon(\lambda)$  and thus of the particle plasmon resonance also dictate a spectral variation of  $\gamma_{rad}(\lambda)$  and  $\gamma_{nr}(\lambda)$ . The different reference points  $r = 0$  for  $\gamma_{rad}$  and  $K$ , and  $r = a$  for  $\gamma_{nr}$  lead to an intersection of the distance dependence curves of the enhancement and dissipation values. As a result, there exists a maximum of  $S_f$  at a finite distance from the surface whereas  $\gamma_{tot}$  will increase monotonously.

### III. EXPERIMENTAL

The experimental setup is described in detail in Refs. [35] and [11]. It was designed to provide full control over the relative displacement  $\mathbf{r}$  between a single molecule placed on a substrate and the extremity of a tip. We used a home-built scanning probe microscope based on shear-force distance control [60, 61] mounted on an inverted optical microscope. Single-molecule samples were prepared from a dilute solution of terrylene and para-terphenyl (pT) in toluene that was subsequently spin coated onto a microscope slide according to the procedure described in Ref. [62]. The solution crystallizes into a film that can be as thin as about 15 nm in height with well dispersed terrylene molecules that assume a polar angle of  $\alpha = (15 \pm 5)^\circ$  [63, 64] along the  $c$ -axis of pT (see fig. 2). Terrylene turns out to be remarkably photostable in this sample, allowing long term and repeated measurements on the same single molecule [62]. Furthermore, terrylene has a quantum yield near unity [63].

For illumination and collection we used an immersion objective (Zeiss, NA 1.4) in different quickly switchable modes. We investigated the plasmon resonances of gold nanoparticles using dark field illumination from a Xe arc-lamp and a spectrometer with a cooled CCD detector. Excitation was typically achieved in total internal reflection mode which produced an axial polarization in the focal plane for p-polarized light. For lifetime measurements by time correlated single photon counting [65] we used a single photon avalanche diode (SPAD) and laser pulses of  $< 30$  ps duration at repetition rates of 5 – 75 MHz. Alternatively we could switch to a cooled imaging CCD camera

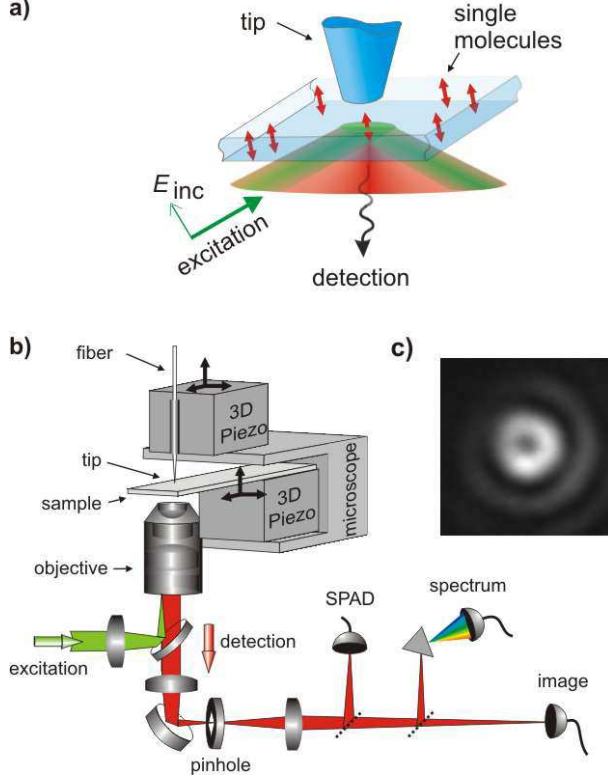


FIG. 2: a) Schematic arrangement of the experiments discussed in this article. A tip is scanned across a thin sample containing single molecule. b) The experimental setup consisting of the scanning stages for the tip and the sample. c) Far-field fluorescence image of a single terrylene molecule. The doughnut emission pattern is a signature of the nearly vertical orientation of the terrylene molecules in the sample.

to record the spatial emission pattern at a system magnification of 230 [66].

Typical experiments started with the imaging of single molecules in wide-field mode to establish their orientation and signal strength  $S_0$ . A single molecule was then selected by closing a pinhole of variable size located in an intermediate image plane. Eventually, a tip was approached and scanned over the stationary sample at distances down to 2 nm from the surface. At each scan pixel, fluorescence intensity and lifetime were recorded simultaneously.

## IV. RESULTS AND DISCUSSION

### A. Single molecules and dielectric tips

The simplest treatments of the modification of spontaneous emission consider perfect metallic mirrors [67], but since real metals absorb in the visible domain, the fluorescence behavior of an emitter is also affected by quenching. In order to avoid this complication, one can use dielectric

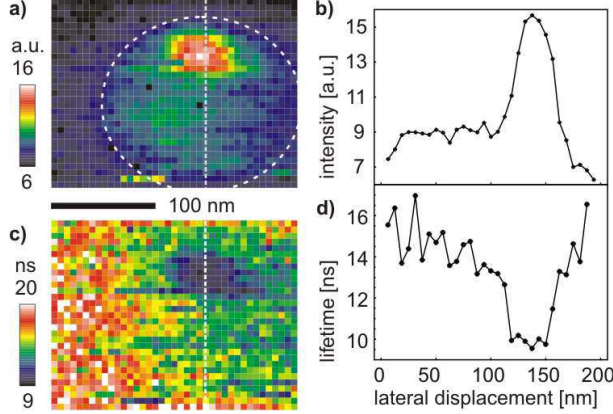


FIG. 3: a) Fluorescence near-field image of a single molecule using a glass tip. b) Cross-section as indicated. c) Map of the lifetime corresponding to image a). d) Cross-section as indicated.

mirrors [52] or nanostructures [6]. Indeed, a number of groups have studied the effect of various dielectric tips on single emitters. While some researches [68, 69] have reported quenching of fluorescence, others have observed enhancement [70, 71]. In this section, we report on well-controlled experiments on aligned single molecules and a glass tip. We show that a simple theoretical model provides a satisfactory agreement with our measurements and indicates the importance of the orientation of the molecule in the modification of its fluorescence under a tip. Details of these investigations can be found in Ref. [12].

A bare heat-pulled glass tip was approached and scanned over a single terrylene molecule embedded in a thin pT film in constant gap mode. The resulting map of the fluorescence signal  $S_f$  is shown in fig. 3a). We can identify two regions where the tip causes  $S_f$  to increase: an area of  $150 \times 150 \text{ nm}^2$  with moderate enhancement indicated by the white circle and then a sharp increase by a factor of 2 in  $S_f$  over  $35 \times 35 \text{ nm}^2$  in the upper part of this circle. The presence of these two distinct regions can be attributed to the tip morphology. Tips created by the heat-pulling process can exhibit plateaus of 50 – 300 nm in size depending on the pulling parameters and sometimes carry spikes of several 10 nm. Both plateau and spike act as polarizable nano-objects and thus increase the excitation rate of the molecule by  $K$ . In the absence of absorption and far below saturation this translates into a proportional increase of  $S_f$  according to eqn. 1. We note that the high collection efficiency  $\xi_0 \approx 75\%$  implies that  $\xi(\mathbf{d}, \mathbf{r})$  does not play a significant role in the observed enhancement [11]. The different magnitudes of  $K$  can be partly attributed to a difference in shape and partly to the gap by which the plateau of the tip is separated from the molecule due to the presence of asperity. Sharp features generally give rise to stronger enhancements than dull



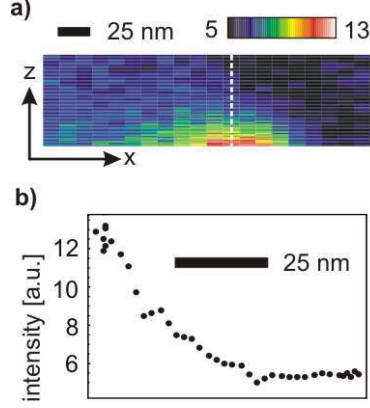


FIG. 4: a) A  $xz$  section of the enhancement landscape taken by approaching the tip to a single molecule. b) Intensity trace when the tip is approached in  $z$  as indicated in a).

ones [71] due to a stronger lightning-rod effect.

The dependence on the vertical separation between the tip and the molecule is displayed in fig. 4a) where a glass tip is repeatedly approached to a terrylene molecule in  $\hat{z}$  at different lateral separations  $y$ . As seen from a cross section of this data in fig. 4b), the enhancement is only significant within the last 15 nm from contact. This fact provides a direct evidence for the strong distance dependence of the near fields close to a polarizable object and supports our interpretation of the lateral scan image.

During the scan we also recorded the excited state lifetime  $\tau = \gamma_{tot}^{-1}$  (see fig. 3c)). The fluorescence lifetime drops from 18 ns for a single molecule embedded in a thin film to 16 ns in the larger area and down to 9 ns in the upper part. Given that glass has a negligible absorption at the molecular emission wavelength, the shorter lifetime is a direct evidence for the accelerated radiation and can be interpreted as an antenna effect [72, 73]. We emphasize, however, that below saturation this increase does not cause a change in  $S_f$ , which is limited by the excitation rate. Thus, the simultaneously observed increase of fluorescence in fig. 3a) is due to the enhancement of  $K$ .

The magnitudes of the enhancement and lifetime change are well reproduced in a model where we approximate the tip by a glass sphere that has a diameter of 100 nm and a refractive index of 1.5. In this simple treatment, we disregard the interface of pT and air and let the system be illuminated by a plane wave along  $\hat{x}$ . For the emission we choose the main peak in the terrylene spectrum at 580 nm. Using the formalism described above, we have evaluated the excitation enhancement  $K$ , the decay rates  $\gamma_{rad/nr}$  and the quantum yield  $\eta$  as a function of the vertical molecule-tip separation  $z$  [55]. The broken lines in figs. 5a) and b) show the results for a molecule oriented perpendicular

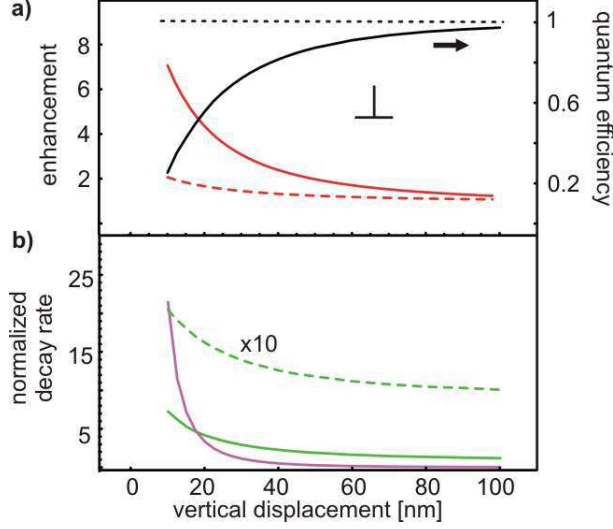


FIG. 5: Emission properties of a dipole placed close to a sphere at radial orientation. Dipole emission wavelength: 580 nm, sphere diameter: 100 nm, material: chromium - *solid lines*, glass - *broken lines*. a) Fluorescence enhancement (*red lines*) and quantum yield (*black lines*). b) Radiative (*green*) and non-radiative (*pink*) decay rate normalized to the free dipole.

to the surface. In the absence of absorption  $\eta$  (black line) remains constant throughout.  $K$  and  $\gamma_{rad}$  (red and green curves) increase by up to a factor of 2 at a distance  $z = 10$  nm. The lateral extent of the enhancement roughly corresponds to the radius of the particle. It is quite remarkable that this simple model predicts the experimentally measured values quite accurately.

We also applied the formalism to a tangentially oriented molecule. The results are shown in figs. 6 a) and b), again as broken lines. Here the model predicts a mild decrease in the excitation rate which means suppression of  $S_f$  to about 70%. Thus, it is the orientation of the molecule that decides if a near-field image with a dielectric tip will show enhancement or inhibition. The difference for the two orientations can easily be illustrated in a simple picture where the molecular dipole interacts with its image dipole. The situation changes, however, if the tip material starts to absorb [74] as is the case for metals.

### B. Single molecules and metallic extended tips

Metallic structures are particularly attractive for modifying fluorescence properties of emitters because they have large dielectric constants  $|\epsilon(\omega)|$ , leading to a strong lightning-rod effect [75]. For chromium,  $\epsilon \approx -8.5 + 29i$  [76] leads to an increase by a factor of 20 compared to glass in the limit of an infinitely thin needle [77]. However, this gain in excitation can be overshadowed by

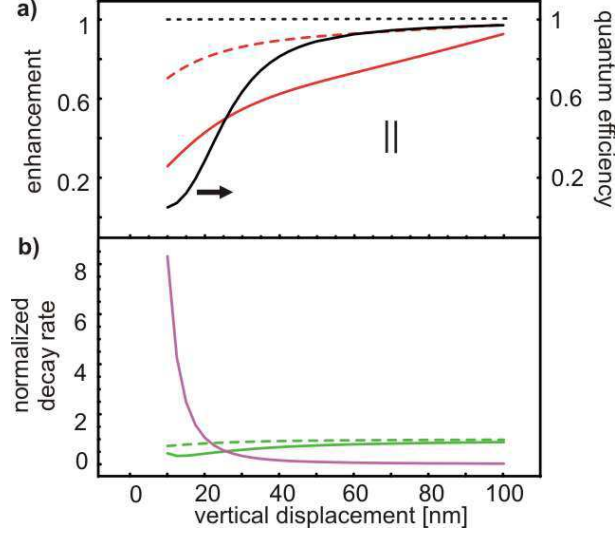


FIG. 6: Emission properties of a dipole placed close to a sphere at tangential orientation. parameters as in fig. 5, material: chromium - *solid lines*, glass - *broken lines*. a) Fluorescence enhancement (*red lines*) and quantum yield (*black lines*). b) Radiative (*green*) and non-radiative (*pink*) normalized decay rate.

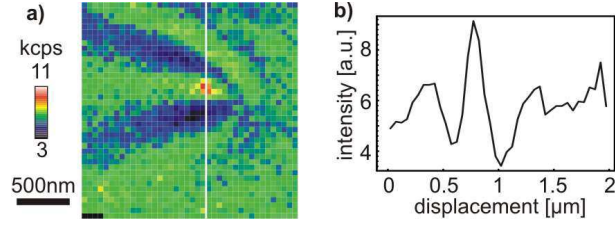


FIG. 7: Single molecule fluorescence near-field images in constant-gap mode for a chromium coated tip. Molecule oriented normal to the scanning plane (terrylene in para-terphenyl).

quenching caused by the imaginary part of  $\epsilon$  [56, 78]. The shape of the structure, the orientation of the molecule and their separations determine the final fluorescence modification.

Metallic tips have been used in many near-field experiments [34, 79, 80]. In our work, we metalized heat-pulled glass tips by head-on thermal evaporation of 30 – 40 nm of chromium. Figure 7a) shows an image of  $S_f$  in the same fashion as for the glass tip. A cross section of this image is provided in fig. 7b) for a quantitative scrutiny. Two features can be distinguished: a sharp peak of 150 nm in full width at half maximum and a far-field interference pattern. The fluorescence enhancement amounts to only 1.6.

Next we exchanged the sample with a thin film of PMMA [107] doped with randomly oriented DiI molecules [108] and switched to the confocal mode of excitation with linearly polarized light. This allowed us to select a dipole oriented in the substrate plane. In this configuration we obtained

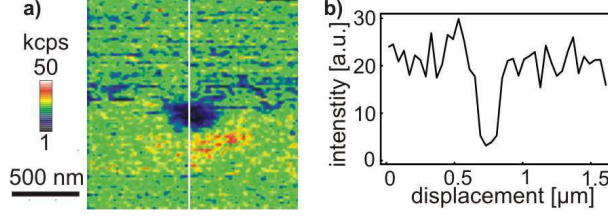


FIG. 8: Single molecule fluorescence near-field images in constant-gap mode for a chromium coated tip. Molecule oriented in the scanning plane (DiI in PMMA).

the image shown in fig. 8a) where complete quenching occurs within a region of 160 nm as the tip meets the molecule. The remaining signal (see fig. 8b)) is caused by residual luminescence from the polymer and the tip. The interference pattern is now absent in the confocal excitation.

The simple model of a Mie particle can be used to explain these observations. We again choose a sphere of 100 nm but now with the dielectric constant of chromium. The results are displayed by the solid curves in fig. 5a) and b) for radially and in fig. 6a) and b) for tangentially oriented dipoles, respectively. In the first case we note a moderate excitation enhancement up to  $K \approx 7$  at a separation of 10 nm. At the same time the quantum yield drops to  $\eta \approx 20\%$  and thus we estimate an overall fluorescence enhancement on the order of  $S_f \approx 1.4$ . Already at a distance of 19 nm the ratio between  $\gamma_{rad}$  and  $\gamma_{nr}$  reverses in favor of the non-radiative decay, diminishing  $\eta$ . Depending on the precise distance,  $S_f$  may rise above or drop below  $S_0$ . The situation is different for the tangential orientation where both  $K$  and  $\eta$  fall below their initial values at any distance  $z$ . Particularly, at  $z \approx 10$  nm we estimate  $S_f \approx S_0/80$  [12]. The interference between the incident and the scattered fields is now destructive on the surface of the sphere so that the resulting tangential field nearly vanishes as would be expected for a perfect metal. By the same token radiation from the molecule is reduced close to the sphere. This inhibition does not necessarily mean quenching but merely a longer lifetime although in the presence of non-radiative decay there will always be quenching.

In the last two sections we have considered the effect of a sharp dielectric or metallic object on the fluorescence of a single molecule. In each case, the orientation of the molecule with respect to the tip axis plays a central role. In the tangential orientation fluorescence will always drop in the near field of a tip whereby its magnitude will depend on the presence of absorption in the tip. For the vertical orientation, enhancement will occur for dielectric tips, but quenching will extinguish the fluorescence at small separations from metallic tips. The tips discussed so far can be considered as lightning rod antennas without any resonances.

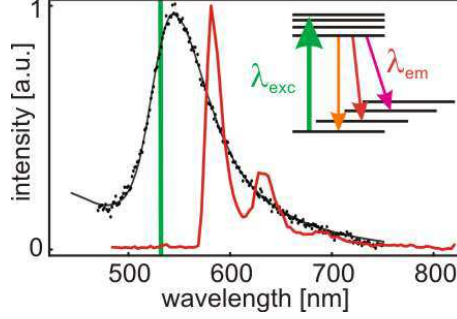


FIG. 9: The plasmon resonance of the nanoparticle (*black*) partially overlaps the emission spectrum of a terrylene molecule (*red*). Possible emission pathways are illustrated in a Jablonski-diagram. The green line indicates the excitation wavelength.

### C. Single molecules and metallic nanoparticles as resonant dipole antennas

Tips and even lithographically fabricated nanostructures vary substantially from one realization to the next. Furthermore, it is a very demanding task to characterize a given nanostructure so that one can account for its geometrical features in a theoretical model. Finally, extended tips are not expected to have well-defined plasmon resonances in the optical domain. To get around these difficulties, a few years ago we initiated a series of experiments where individual colloidal particles are carefully selected and examined via plasmon resonance spectroscopy and tomography [23, 35]. By attaching a single gold particle to the end of a glass fiber tip, we could examine the modification of its plasmon spectrum close to surfaces [63, 81] and investigate the influence of the particle on the fluorescence of single fluorescent molecules [11]. In the next sections, we discuss our results from the latter system. In particular, we provide direct studies of the enhancement of the excitation at particle plasmon resonance, modification of the molecular fluorescence lifetime and its emission spectrum, and the tip's strong influence on the emission pattern of the molecule.

#### 1. Fluorescence enhancement and quenching

Gold particles of  $a = 50$  nm were attached to glass tips following the procedure of Ref. [35]. We repeatedly monitored the scattering spectrum (see fig. 9) during the experiment as a sensitive indicator of the well-being of the tip. Single molecules were identified in a wide-field excitation arrangement and using a sensitive CCD camera. An example of the radiation pattern of a single molecule is shown in fig. 2c).

Once a molecule was selected, its fluorescence was directed to an avalanche photodiode and the

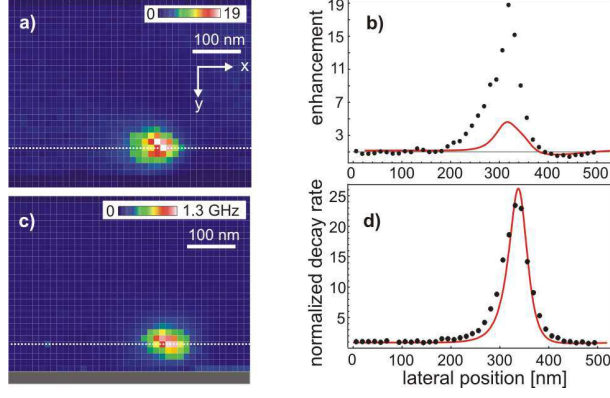


FIG. 10: Single molecule near-field image with a resonantly excited gold-nanoparticle. a) Map of the fluorescence intensity  $S_f$ . b) Cross-section from a). c) Corresponding map of the excited state decay rate  $\gamma$ . d) Cross-section from c). Calculations of  $S_f/S_0$  and  $\gamma/\gamma^0$  are also displayed as solid red lines in (b) and (d).

gold particle was scanned close to the sample surface. The near-field images of a single molecule shown in fig. 10 were obtained with pulsed excitation light of 532 nm. The fluorescence intensity  $S_f$  typically exhibits a sharp rise over a region of  $60 \times 60 \text{ nm}^2$  as the tip comes close to the molecule. From the signal  $S_0$  of the unperturbed molecule (blue shade) we deduce an enhancement factor of 19 (fig. 10b)) after carefully subtracting the residual luminescence  $S_b$  from the tip and the sample substrate [11]. In other measurements (over many months, including many samples and many tips) we have obtained enhancement factors ranging between 10 and 32. These variations are caused by different depths  $z_{min}$  of the molecules in the film (see below). We point out a slight asymmetry in the peak shape and the slight suppression of the signal at  $x \approx 440 \text{ nm}$ . These are due to the tilt of the molecule and to interference effects discussed in Ref. [11] and its EPAPS Supplementary Material.

An important advantage of our experiment is that we have also recorded the molecular fluorescence lifetime at every scan pixel simultaneously as the fluorescence intensity. The corresponding map of the decay rate is shown in fig. 10c). Again a region of accelerated decay can be seen with similar lateral extensions. The decay rate  $\gamma = \tau^{-1}$  is found to peak at about 22 times the unperturbed value. We again note a slight asymmetry in the cross-section shown in fig. 10d) produced by the tilt of the molecular dipole moment[11, 82].

A close examination of the scan images in figs. 10a) and c) reveals a slight systematic offset between the two enhancement spots. To help the visualization of this interesting effect, in fig. 11a) we show the superposed contour plots of these two quantities from several molecules but the same

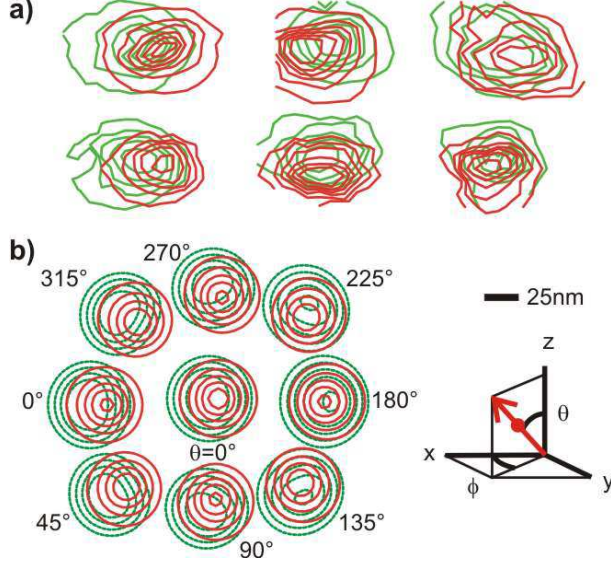


FIG. 11: a) Contours of constant enhancement (green) and decay rate (red) for five different molecules. b) Calculated contours for different azimuthal orientations of the molecular dipole  $\phi$  at  $\theta = 15^\circ$  as defined in the inset.

gold nanoparticle. The points of highest enhancement and fastest decay rate are typically displaced from one another by up to  $\Delta x = 20$  nm. The direction of the displacement, however, varies for different molecules. We have presented the detailed analysis of this issue in the supplementary materials of Ref. [11]. In a nutshell, as the particle moves across the molecule, the relative orientation of the molecular dipole changes with respect to the gold sphere. Since tangential and radial orientations result in completely different excitation enhancement and fluorescence lifetime modification behaviors, a slight tilt of the molecule (about  $15^\circ$  for terrylene in pT [62]) causes a notable asymmetry between the intensity and lifetime images.

As discussed in the supplement of Ref. [11], having a good estimate of the separation between the molecule and the particle and knowing the tilt of the molecular dipole, we can calculate the modification of the excitation intensity at the position of the molecule, of its radiative and nonradiative decay rates and thus its quantum efficiency. Based on these calculations, we have plotted the expected profile of the detected fluorescence by the red curve in fig. 10b). The spatial extent of the enhancement region and its asymmetric shape agree well with the predictions of theory apart from a slight broadening in the wings of the experimental curves. However, the magnitude of  $S_f$  falls short by a factor of 2-3 compared to the experimental values. This implies that  $K$  and/or  $\eta$  are larger for the true geometry than in the simplified model [83]. We point out, however, that an accurate description of the system must account for pT-air interface [84, 85] as



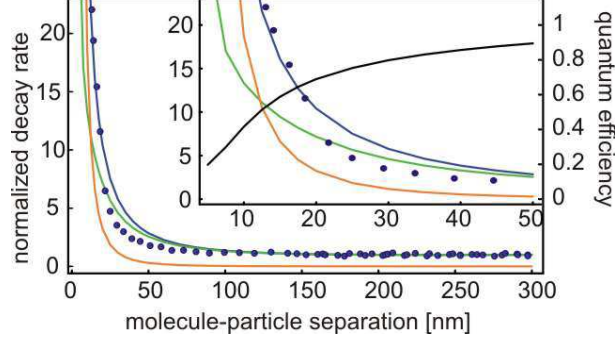


FIG. 12: Fluorescence decay rate for a  $\hat{z}$  approach. The symbols show the experimental decay rate  $\gamma_{tot}$  and the lines give the calculated values of  $\gamma_{rad}$  (orange),  $\gamma_{nr}$  (red) and  $\gamma_{tot}$  (blue). Inset: magnified plot with quantum yield  $\eta$  (black).

well as the evanescent mode of excitation for the tip.

It is also instructive to examine  $K$  and  $\gamma$  as a function of the molecule-particle separation in the  $z$  direction. As shown by the pink curve in fig. 12b), calculations predict an increase in both  $\gamma_{rad}$  and  $\gamma_{nr}$  as  $z$  is decreased, but  $\gamma_{nr}$  is expected to dominate at very small distances. The blue symbols in the experimental data show the measured total decay rate as the particle was approached to the molecule [11]. The agreement with the blue curve, which is the sum of the pink and green plots, is very good except for a slightly weaker decay around  $z \approx 50$  nm. Nevertheless, it is apparent that  $\gamma_{nr}$  starts to dominate at  $z \leq 12$  nm and leads to a decline of  $\eta$  (inset). Equality of  $\gamma_{rad}$  and  $\gamma_{nr}$  marks the point of  $\eta = 50\%$ . At distances  $\leq 5$  nm the signal  $S_f$  is expected to fall below its original value  $S_0$ . In this experiment, the tip could not be approached closer to the molecule because of the finite depth of the latter in the sample. In fact, in our system the great majority of molecules that are very close to the upper surface tend to bleach, most probably due to residual or inter-diffusing oxygen [86, 87].

In order to explore the complete three dimensional near-field interaction of a gold particle and a single molecule, we have also scanned the tip in the  $xz$  plane at different  $y$ 's. The experimental data is presented in the first and the third rows of fig. 13a). Here  $S_f$  reaches an absolute maximum enhancement of 17 when the tip assumes the smallest separation  $z_{min}$  from the sample surface for  $y = 0$ . A selection of approach curves from the  $y = 0$  data is shown in fig. 13b). When the  $x$ -separation between the particle and the molecule is large (lower graphs), only a slight quenching occurs for small  $z$ . As the particle comes closer to the molecule in the  $x$  direction (top graphs), the fluorescence is first enhanced but it then reaches a maximum and turns around at about 5 nm. This effect has been also reported in Ref. [88]. We also note that for some  $y$  values (e.g.



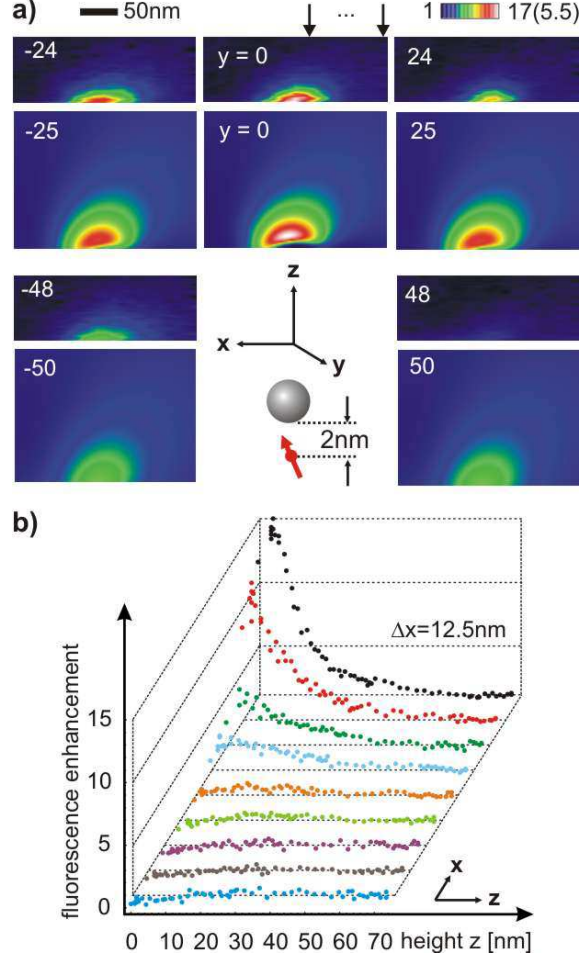


FIG. 13: a) First and third row:  $xz$  section scans of  $S_f$  at different constant coordinates  $y$  as given above (in nm). Second and fourth row: calculation of  $S_f(x, z, y = \text{const})$  for a dipole that is tilted by angle  $\alpha = 25^\circ$  toward  $\hat{x}$  and  $z_{\min} = 2\text{nm}$ . b) A selection of vertical cross sections from the  $y = 0$  image, as indicated by the arrows in a).

$y = 24\text{ nm}$ ),  $S_f$  assumes its maximum value at a distance  $z > z_{\min}$  (see fig. 13a)). This phenomenon is more clearly seen in the calculations that are plotted in the second and fourth rows of fig. 13a) below each corresponding experimental image. Furthermore, the skewed elongated character of the experimental regions of enhancement is reproduced in the calculations with a nearly quantitative agreement. We mention, however, that in these calculations a better agreement was obtained with the experimental data when we chose an inclination angle of  $\alpha \approx 25^\circ$  toward  $\hat{x}$ .

The data in fig. 13 let us predict that for a normally oriented molecule and a small tip-sample

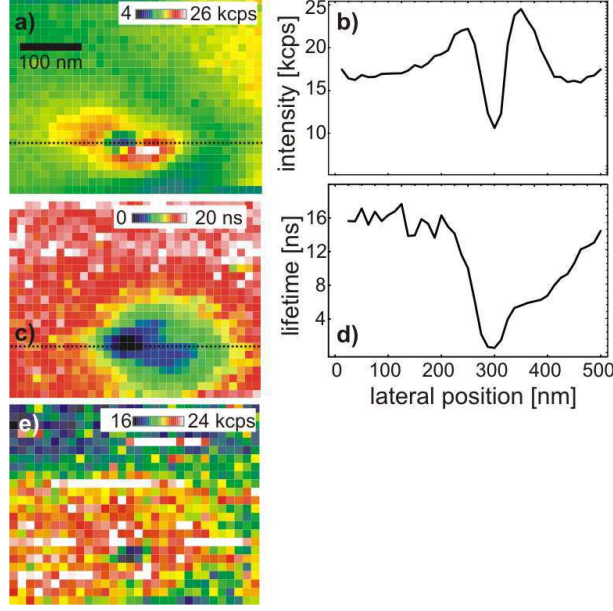


FIG. 14: a) Fluorescence signal  $S_f$  for a near-field scan with a gold nano-particle at minimal  $z_{min}$  and excitation wavelength  $\lambda_{exc} = 532$  nm. b) Cross-section from a). c) Map of the lifetime  $\tau$  recorded simultaneously with a). d) Cross-section from c). e) Same as a) but with  $\lambda_{exc} = 488$  nm.

separation, we can expect a dip in the center of the image due to a pronounced quenching (see the  $y = 0$  data set in the second row of fig. 13a)). For large  $z_{min}$  or tilted molecules the enhancement will have a central maximum as in fig. 10 and possibly a weak minimum. The data in fig. 14 show lateral scans of  $S_f$  and  $\tau$  at very small particle-molecule separations where quenching becomes very important. A significant drop of about 50% in the fluorescence rate  $S_f$  (see fig. 14b)) coincides with a drop in the lifetime  $\tau$  from 16 ns to below 1 ns in fig. 14d). The central quenching pit in fig. 14a) is flanked by a circular region where the fluorescence is enhanced by 1.5 times. The corresponding map of the lifetime shown in fig. 14c) and d) exhibits a steep rise to the left and a slower recovery with a shoulder to the right from the main quenching spot. The fact that both lifetime and fluorescence signals drop is indicative of quenching. We mention that a small dip of the fluorescence enhancement at the center of lateral scans has been also reported in Ref. [88] but corresponding lifetime measurements were missing.

The strong enhancement discussed here was explained via the optical properties of a gold nanoparticle using the same formalism as for a glass or chromium spheres treated earlier. An important and decisive feature of a gold nanoparticle is that it supports a plasmon resonance, making it behave like a "resonant optical antenna" [89, 90, 91]. In the next two sections we discuss the role of the plasmon resonance on the molecular excitation and emission processes.

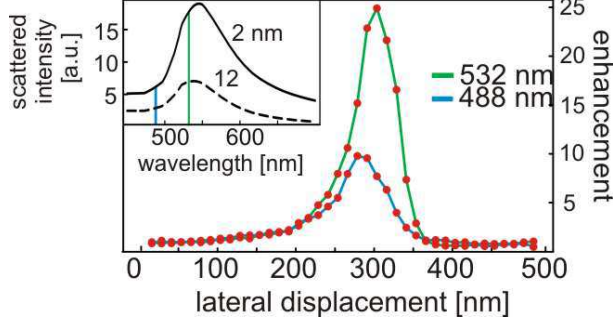


FIG. 15: Comparison of the enhancement at resonant (*green*) and non-resonant (*blue*) excitations. The inset shows a calculation of  $K(\lambda_{exc})$  at distances of 2 and 12 nm.

### 2. The role of plasmon resonance in the molecular excitation

As shown by the spectrum in fig. 9, the plasmon resonances of the nanoparticles we studied show a maximum around 550 nm but a minimal scattering response close to 490 nm. This means that also  $K$  should depend on the wavelength of excitation. We have compared the fluorescence signals  $S_f$  for the excitation with blue (488 nm) and green (532 nm) light. To keep all other parameters constant, we combined the two colors on the same optical path and switched between the sources during a raster scan. The images thus acquired resemble those of fig. 10. However, the enhancement with the blue light is smaller by a factor of 2.5 as can be seen from a line scan shown in fig. 15 [11]. The difference between the maxima of  $S_f$  is fully attributed to  $K$  since the conditions for the emission of the molecule remain unaltered. The inset shows calculations for  $K(\lambda)$  or equivalently, the near-field plasmon resonance at  $z = 2$  and 12 nm. An enhancement ratio of 2.5 corresponds to  $z = 8$  nm.

Another interesting effect is shown in fig. 14e) where the fluorescence intensity of the same molecule as in fig. 14a) is plotted but this time under excitation at 488 nm. Under the weaker excitation at this wavelength the circular region of enhancement that was observed for green excitation is absent and only the central quenching pit remains.

### 3. The role of plasmon resonance in the molecular emission Spectrum

According to Fermi Golden Rule  $\gamma_{rad}(\omega)$  is proportional to the photonic density of states  $\rho(\omega)$  [77, 92]. Similar to the case of an emitter placed close to a perfect mirror, the density of states and thus  $\gamma_{rad}$  are expected to be modified for emitters close to resonant nanostructures [9, 53, 93]. Above, we have provided experimental data for the change of the total fluorescence decay rate and

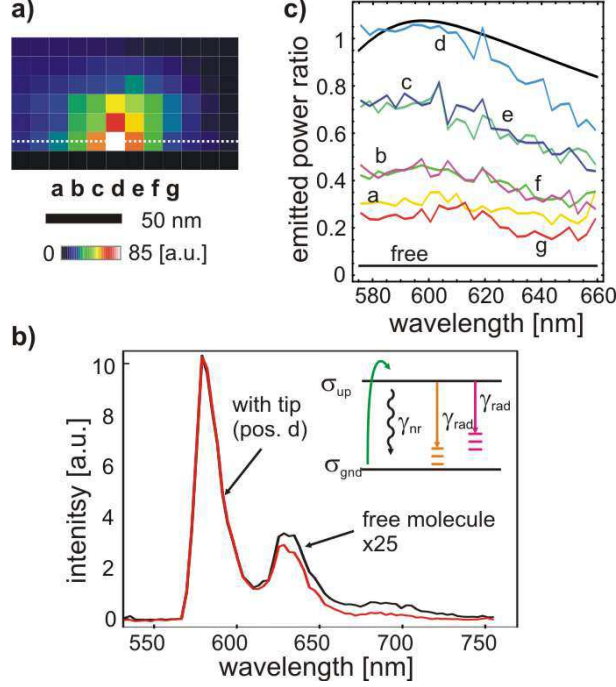


FIG. 16: a) Map of the integrated fluorescence intensity as the gold particle is scanned across a terrylene molecule. b) Normalized fluorescence spectra of the unperturbed molecule (black) and at maximal enhancement (pixel "d" of the line indicated in a). c) Ratio of the spectra measured at pixels a-g to the unperturbed molecule.

have discussed theoretical calculations that help us estimate how much of this observed change is due to  $\gamma_{\text{rad}}$  as opposed to  $\gamma_{\text{nr}}$ . A direct experimental measurement of these two parameters remains the topic of a future publication [83]. However, here, we give direct evidence for the modification of  $\gamma_{\text{rad}}$  through the change of the emission spectrum.

To investigate the modification of the molecular emission spectrum under the influence of a gold nanoparticle, we have recorded the fluorescence spectrum of a single molecule using a grating spectrometer as the tip was scanned across the molecule. The integrated spectra are shown in fig. 16a), constituting a total near-field image  $S_f$ . In these measurements, the enhancement reached a factor of 25 just before the molecule underwent photobleaching. In fig. 16b) we show the normalized spectrum for the most intense pixel labeled "d" in fig. 16a) (red curve) and the spectrum of the same unperturbed molecule (black curve). It is evident that the enhanced spectrum falls below the reference spectrum at longer wavelengths (630 – 750 nm).

The fluorescence spectrum of terrylene in fig. 16 shows three peaks due to the emission from the lowest vibrational state of the electronic upper state to different vibrational levels of the electronic ground state (see the inset in fig. 9). The spectral power density  $p(\lambda)$  is proportional to  $\sigma_{\text{up}}\gamma_{\text{rad}}(\lambda)$

where  $\sigma_{up}$  denotes the common upper state population. Although we do not know  $\sigma_{up}$  in the absence and presence of the gold particle, because it is the same for all emission channels, we can probe the effect of  $\gamma_{rad}(\lambda)$  by comparing the fluorescence enhancement at different wavelengths. To do this, we have computed the ratio  $\gamma_{rad}^{gold}(\lambda)/\gamma_{rad}^{free}(\lambda)$  by dividing the spectra obtained with and without the gold particle. This ratio is shown in fig. 16c) for a selection of pixels in fig. 16a). The imbalance in the emission enhancement increases gradually as the distance between the molecule and nanoparticle decreases. At the maximum of fluorescence intensity (curve d in fig. 16c) we find that the highest emission enhancement is assumed around 600 nm, i.e. red-shifted from the scattering resonance at 550 nm [9, 85]. The overall tendency of the experimental data is in a reasonable agreement with the theoretical ratio of  $\gamma_{rad}^{gold}(\lambda)/\gamma_{rad}^{free}(\lambda)$  plotted by the black curve in fig. 16c).

From these results we can conclude that it is crucial to consider the optical properties of the material in the design of an optical antenna [90, 94]. The material non-idealities compared to radio frequencies alter the relation between the antenna resonance and shape. Excitation enhancement and emission efficiency cannot be related by simple reciprocity arguments but have to account for absorption [41].

#### 4. Radiation pattern

Antenna design aims at connecting *localized* sources and detectors through specific directional characteristics. A dipole, however, radiates nearly isotropically. Efficient excitation and collection requires high-grade optics that are not viable in many applications. To improve the directionality from a molecule, it has been proposed that reflectors and directors using the Yagi-Uda principle can be used [95, 96]. It turns out that a single nanoparticle can also alter the radiation pattern of the molecule. Indeed, the modification of angular emission due to a solid near-field tip has been reported [97].

To investigate the radiation pattern from a single molecule in the presence of a nano-antenna, we directed the emitted light at high magnification onto an imaging CCD camera. The beam produced by an aberration-free microscope objective is the transform of the radiation pattern  $I(\theta, \phi)$  at the focal plane according to  $I(\rho, \phi) \propto I(\theta, \phi)/\cos \theta$  with  $\rho = f \sin \theta$  where  $f$  is the effective focal length [98]. An axially oriented dipole thus produces a radially polarized doughnut-shaped distribution [62, 66] (see fig. 2d). In case of terrylene embedded in para-terphenyl there exists also a slight asymmetry due to its tilt [62].

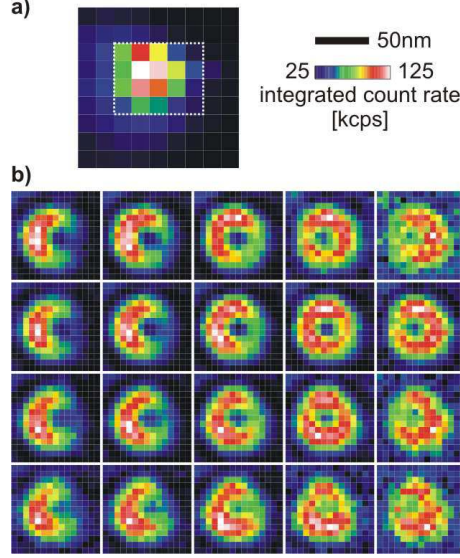


FIG. 17: a) Integrated intensity map for a near-field scan of a gold particle across a terrylene molecule. b) Radiation pattern on the CCD camera for a set of displacements corresponding to the 20 pixels within the white box in a).

We have collected a sequence of such images as the nanoparticle was scanned across a molecule. As before, the integrated count rate on the camera produces a typical enhancement map shown in fig. 17a), with a maximum of 25 in this scan. Figure 17b) shows the spatially resolved camera images for the tip locations corresponding to the pixels within the white square in a). Inspection of these images reveals a redistribution of the intensity going from a “waning” to a “waxing” crescent in the first and last columns, respectively. Similarly, for the top and bottom rows the bright regions can be found in the upper and lower sections of the doughnut. A simple trend is obvious: the weight of the intensity in the pattern follows the direction of displacement of the tip.

To explain the redistribution of power, we have calculated the radiation pattern for a dipole close to a gold sphere [55] at different locations. Cross-sections of this pattern in the  $xz$ -plane are shown in fig. 18. The model predicts an inclination of the radiation pattern towards the line connecting sphere and molecule [41]. This is a consequence of the radial component of the molecular dipole which polarizes the sphere to produce a large common dipole moment. The emission from the tangential component remains inferior in our geometry. It merely produces a slight right-left asymmetry and most notably the alleviation of the pinch-off at  $x = 50$  nm. We note that our calculation does not represent the true geometry including the pT interface [99, 100], which directs almost the entire radiation into the higher index medium. The change of the emission pattern shows the necessity for a high collection solid-angle and implies that the excitation conditions

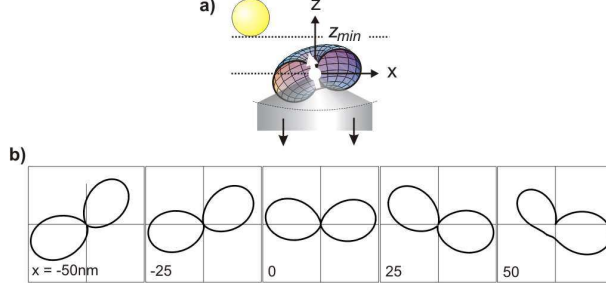


FIG. 18: Calculated radiation pattern for the dipole - gold sphere system. a) Model schematic with the parameters:  $\alpha = 15^\circ$ ,  $z_{min} = 10$  nm. b) Radiation pattern of a molecule in the presence of a gold sphere with displacement  $x = (-50...50)$  nm. The total power emitted at any point is given by the intensity map according to fig. 10.

should be in principle optimized for each given separation  $\mathbf{r}$ . By using of the reciprocity theorem, we can predict that the excitation beam should be shaped similar to the radiation pattern. Optimal excitation can therefore be achieved with a radially polarized doughnut beam [85, 101].

#### D. Optimizing antenna structures

In the previous sections, we have shown that a gold nanoparticle acts as a nano-antenna to enhance the fluorescence signal of single emitters. However, we also showed that absorption of light by the gold particle causes quenching so that one cannot harvest the greatest excitation and spontaneous emission enhancements at very small separations. The question that arises is then if one could devise an arrangement for achieving a very high spontaneous emission rate without sacrificing the quantum efficiency. Furthermore, it would be desirable to achieve more significant enhancement of excitation than was possible from a nanosphere. We have recently tackled this problem theoretically for simple antenna geometries of two nanoparticles [9]. Using full electrodynamics simulations [102], we have applied some simple design rules to nanoantennae made of two prolate spheroidal gold particles as sketched in fig. 19a). Due to the lack of space, we refer the interested reader to Ref. [9] for a detailed discussion of this topic. Here it suffices to state that by varying size, aspect ratio, distance and background medium, we have found that quenching can be avoided to a large extent. Moreover, radiative decay enhancements up to three order of magnitudes can be achieved in the near-infrared spectral range [9, 57, 103]. By invoking reciprocity, we conclude that this enhancement also applies to the near field and thus to the excitation process, as previously pointed out in the literature [104].

Although we expect the best results for the near-infrared emitters, it is possible to optimize the



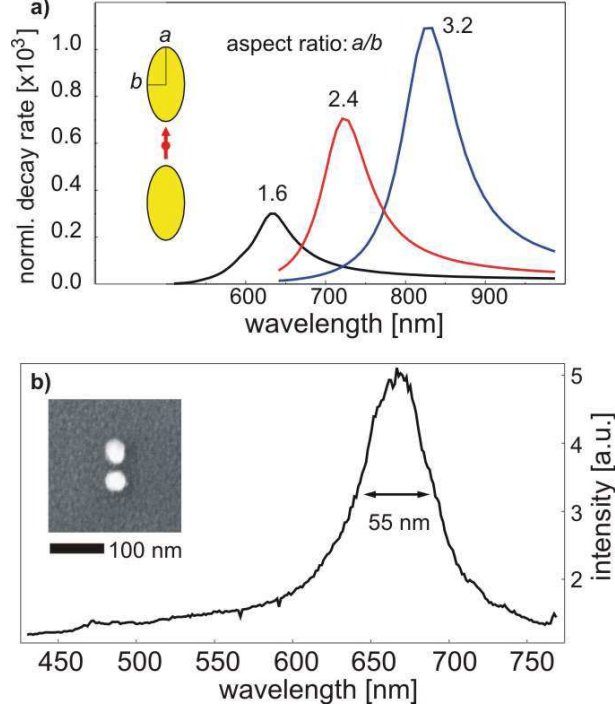


FIG. 19: a) Normalized radiative decay rate as a function of the NPs aspect ratio  $a/b$  for an emitter coupled to the gold nanoantenna as shown in the inset. NPs details: aspect ratio 1.6 ( $a=76$  nm,  $b=48$  nm), 2.4 ( $a=100$  nm,  $b=42$  nm), and 3.2 ( $a=122$  nm,  $b=32$  nm). The NPs are separated by about 20 nm and are embedded in a medium with refractive index equal to 1.3. b) The measured plasmon spectrum of a gold nanoantenna fabricated by electron beam lithography. The incident light is polarized parallel to the nanoantenna long axis. Inset: SEM image of the fabricated sample.

coupling of gold nanoparticles to emitters in the visible range. Figure 19a) describes how the aspect ratio of the nanoparticles can be used to adjust the plasmon resonance to the desired wavelength. The quantum efficiency is close to one and insensitive to the aspect ratio for wavelengths larger than about 750 nm, while it exhibits a rapid drop for shorter wavelengths, depending on the nanoparticle's shape and background medium [57, 103]. Similar trends should be found also for gold nanorods [105].

To close, we briefly present an experimental progress report on the fabrication of double-particle antennae [57]. The inset in fig. 19b) displays a scanning electron microscope image of a nanoantenna fabricated by electron-beam lithography. Such a structure with an overall size around 100 nm is very promising for the realization of a hybrid subwavelength emitter with tailored radiative features. The main part of fig. 19b) shows the plasmon resonance recorded from such a structure [57]. The resonance at 670 nm corresponds to slightly elongated nanoparticles separated by only about 15 nm. From the experimental point of view, the fabrication of the ideal nanoantennae remains a nontrivial



task. Furthermore, proper positioning of a single molecule in the gap between two nanoparticles is quite challenging. Nevertheless, there is no doubt that in the next few years nano-optics will witness a rapid progress in this direction.

### Acknowledgements

We thank F. Robin for fabricating gold nanoantennae at FIRST, the Center for Micro- and Nanoscale Science at ETH Zurich. We thank U. Håkanson, L. Rogobete and F. Kaminski for fruitful discussions. This work was supported by the Swiss Ministry of Education and Science (EU IP-Molecular Imaging), the ETH Zurich initiative on Composite Doped Metamaterials (CDM) and the Swiss National Foundation (SNF).

- 
- [1] A. Sommerfeld, Ann. Phys. (Leipzig) **28**, 665736 (1909).
  - [2] E. M. Purcell, Phys. Rev. **69**, 681 (1946).
  - [3] K. H. Drexhage, Progress in Optics **12**, 165 (1974).
  - [4] P. R. Berman, *Cavity Quantum Electrodynamics* (Academic Press, 1994).
  - [5] R. Chang, W. Fann, and S. H. Lin, Appl. Phys. Lett. **69**, 2338 (1996).
  - [6] C. Henkel and V. Sandoghdar, Opt. Comm. **158**, 250 (1998).
  - [7] L. Rogobete, H. Schniepp, V. Sandoghdar, and C. Henkel, Opt. Lett. **28**, 1736 (2003).
  - [8] A. F. Koenderink, M. Kafesaki, C. M. Soukoulis, and V. Sandoghdar, Opt. Lett. **30**, 3210 (2005).
  - [9] L. Rogobete, F. Kaminski, M. Agio, and V. Sandoghdar, Opt. Lett. **32**, 1623 (2007).
  - [10] H. Schniepp and V. Sandoghdar, Phys. Rev. Lett. **89**, 257403 (2002).
  - [11] S. Kühn, U. Håkanson, L. Rogobete, and V. Sandoghdar, Phys. Rev. Lett. **97**, 017402 (2006).
  - [12] S. Kühn and V. Sandoghdar, Appl. Phys. B **84**, 211 (2006).
  - [13] J. Seelig, K. Leslie, A. Renn, S. Kuhn, V. Jacobsen, M. van de Corput, C. Wyman, and V. Sandoghdar, Nano Lett. **7**, 685 (2007).
  - [14] M. Fleischmann, P. Hendra, and A. McQuillan, Chem. Phys. Lett. **26**, 163 (1974).
  - [15] D. Jackson, *Classical Electrodynamics* (Wiley and Sons, 1999).
  - [16] H. Metiu, Prog. Surf. Sci. **17**, 153 (1984).
  - [17] M. Moskovits, Rev. Mod. Phys. **57**, 783 (1985).
  - [18] J. Gersten and A. Nitzan, J. Chem. Phys. **75**, 1139 (1981).
  - [19] R. Ruppin, J. Chem. Phys. **76**, 1681 (1982).
  - [20] H. Chew, Phys. Rev. A **38**, 3410 (1988).
  - [21] F. Kulzer and M. Orrit, Ann. Rev. Phys. Chem. **55**, 585 (2004).

- [22] T. Klar, M. Perner, S. Grosse, G. von Plessen, W. Spirkel, and J. Feldmann, Phys. Rev. Lett. **80**, 4249 (1998).
- [23] T. Kalkbrenner, U. Håkanson, and V. Sandoghdar, Nano Lett. **4**, 2309 (2004).
- [24] K. Lindfors, T. Kalkbrenner, P. Stoller, and V. Sandoghdar, Phys. Rev. Lett. **93**, 037401 (2004).
- [25] M. A. van Dijk, A. L. Tchegbotareva, M. Orrit, M. Lippitz, S. Berciaud, D. Lasne, L. Cognet, and B. Lounis, Phys. Chem. Chem. Phys. **8**, 3486 (2006).
- [26] S. Nie and S. R. Emory, Science **275**, 1102 (1997).
- [27] K. Kneipp, Y. Wang, H. Kneipp, L. T. Perelman, I. Itzkan, R. R. Dasari, and M. S. Feld, Phys. Rev. Lett. **78**, 1667 (1997).
- [28] W. P. Ambrose, P. M. Goodwin, J. C. Martin, and R. A. Keller, Science **265**, 364 (1994).
- [29] X. S. Xie and R. C. Dunn, Science **265**, 361 (1994).
- [30] S. Kawata and Y. Inouye, Opt. Lett. **19**, 159 (1994).
- [31] F. Zenhausern, M. Oboyle, and H. Wickramasinghe, Appl. Phys. Lett. **65**, 1623 (1994).
- [32] P. Gleyzes, A. C. Boccarda, and R. Bachelot, Ultramicroscopy **57**, 318 (1995).
- [33] A. Hartschuh, E. J. Sánchez, X. S. Xie, and L. Novotny, Phys. Rev. Lett. **90**, 95503 (2003).
- [34] E. J. Sanchez, L. Novotny, and X. S. Xie, Phys. Rev. Lett. **82**, 4014 (1999).
- [35] T. Kalkbrenner, M. Ramstein, J. Mlynek, and V. Sandoghdar, J. Microsc. **202**, 72 (2001).
- [36] J. Wessel, J. Opt. Soc. Am. B **2**, 1538 (1985).
- [37] D. Pohl, *Near-field Optics: Principles and Applications* (World Scientific Publ., Singapore, 2000), chap. Near-field optics seen as an antenna problem, pp. 9–21.
- [38] P. J. Schuck, D. P. Fromm, A. Sundaramurthy, G. S. Kino, and W. E. Moerner, Phys. Rev. Lett. **94**, 017402 (2005).
- [39] P. Mühlischlegel, H.-J. Eisler, O. Martin, B. Hecht, and D. Pohl, Science **308**, 1607 (2005).
- [40] U. Kreibig and M. Vollmer, *Optical Properties of Metal Clusters* (Springer Berlin, 1995).
- [41] M. Thomas, J.-J. Greffet, R. Carminati, and J. Arias-Gonzalez, Appl. Phys. Lett. **85**, 3863 (2004).
- [42] C. Bohren and D. Huffman, *Absorption and scattering of light by small particles* (John Wiley & Sons, Inc., 1998).
- [43] C.-T. Tai, *Dyadic Greens functions in electromagnetic theory* (Intext educational publishers Scranton-San Francisco-Toronto-London, 1971).
- [44] A. Zvyagin and K. Goto, J. Opt. Soc. Am. A **15**, 3003 (1998).
- [45] M. Quinten, A. Pack, and R. Wannemacher, Appl. Phys. B **68**, 87 (1999).
- [46] J. Lock, J. Opt. Soc. Am. A **12**, 929 (1995).
- [47] K. Kelley, E. Coronado, L. Zhao, and G. Schatz, J. Phys. Chem. B **107**, 668 (2003).
- [48] L. J. Richter, C. E. Jordan, R. R. Cavanagh, G. W. Bryant, A. Liu, S. J. Stranick, C. D. Keating, and M. J. Natan, J. Opt. Soc. Am. A **16**, 1936 (1999).
- [49] H. Chew, D.-S. Wang, and M. Kerker, Appl. Opt. **18**, 2679 (1979).
- [50] J. R. Lakowicz, Anal. Biochem. **337**, 171 (2005).

- [51] R. X. Bian, R. C. Dunn, X. S. Xie, and P. T. Leung, Phys. Rev. Lett. **75**, 4772 (1995).
- [52] K. Sullivan and D. Hall, J. Opt. Soc. Am. B **14**, 1149 (1997).
- [53] H. Metiu, Prog. Surf. Sci. **17**, 153 (1984).
- [54] V. Klimov, M. Ducloy, and V. Letokov, J. Mod. Phys. **43**, 2251 (1996).
- [55] H. Chew, J. Chem. Phys. **87**, 1355 (1987).
- [56] P. Das and A. Puri, Phys. Rev. B **65**, 155416 (2002).
- [57] M. Agio, G. Mori, F. Kaminski, L. Rogobete, S. Kühn, V. Callegari, P. M. Nellen, F. Robin, Y. Ekinci, U. Sennhauser, et al. Proc. SPIE, submitted.
- [58] A. Caticha, Phys. Rev. B **62**, 3639 (2000).
- [59] R. Carminati and M. Nieto-Vesperinas, J. Opt. Soc. Am. A **15**, 706 (1998).
- [60] E. Betzig, P. Finn, and J. Weiner, Appl. Phys. Lett. **60**, 2484 (1992).
- [61] K. Karrai and I. Tiemann, Phys. Rev. B **62**, 13174 (2000).
- [62] R. J. Pfab, J. Zimmermann, C. Hettich, I. Gerhardt, A. Renn, and V. Sandoghdar, Chem. Phys. Lett. **387**, 490 (2004).
- [63] B. C. Buchler, T. Kalkbrenner, C. Hettich, and V. Sandoghdar, Phys. Rev. Lett. **95**, 063003 (2005).
- [64] S. Kummer, F. Kulzer, R. Kettner, T. Basche, C. Tietz, C. Glowatz, and C. Krysch, J. Chem. Phys. **107**, 7673 (1997).
- [65] W. Becker, A. Bergmann, M. Hink, K. König, K. Benndorf, and C. Biskup, Microscopy Research and Technique **63**, 58 (2004).
- [66] M. Bohmer and J. Enderlein, J. Opt. Soc. Am. B **20**, 554 (2004).
- [67] S. Haroche, in *Fundamental systems in quantum optics* (North-Holland, Amsterdam, 1992), pp. 767–940.
- [68] W. Tragesinger, A. Kramer, M. Kreiter, B. Hecht, and U. Wild, J. Microscopy **209**, 249 (2003).
- [69] W. Tragesinger, A. Kramer, M. Kreiter, B. Hecht, and U. P. Wild, Appl. Phys. Lett. **81**, 2118 (2002).
- [70] V. Protasenko and A. Gallagher, Nano Lett. **4**, 1329 (2004).
- [71] F. H'dhili, R. Bachelot, A. Rumyantseva, and G. Lerondel, J. Microscopy **209**, 214 (2002).
- [72] Y. C. Martin, H. F. Hamann, and H. K. Wickramasinghe, J. Appl. Phys. **89**, 5774 (2001).
- [73] S. Patane, P. Gucciardi, M. Labardi, and M. Allegrini, Revista del nuovo cimento **27**, 1 (2004).
- [74] R. Chance, A. Prock, and R. Silbey, Adv. Chem. Phys. **37**, 1 (1978).
- [75] A. Ermushev, B. Mchedlishvili, V. Oleinikov, and A. Petukhov, Quant. Electron. **23**, 435 (1993).
- [76] S. R. Lide, *Handbook of Chemistry and Physics*, 75th edn. (CRC Press, 1995).
- [77] V. Klimov, M. Ducloy, and V. Letokov, Quant. Electron. **31**, 569 (2001).
- [78] J. Azoulay, A. Debarre, A. Richard, and P. Tchenio, Europhys. Lett. **51**, 374 (2000).
- [79] Y. Inouye and S. Kawata, Opt. Lett. **19**, 159 (1994).
- [80] A. Kramer, W. Tragesinger, B. Hecht, and U. Wild, Appl. Phys. Lett. **80**, 1652 (2002).
- [81] T. Kalkbrenner, U. Håkanson, A. Schädle, S. Burger, C. Henkel, and V. Sandoghdar, Phys. Rev. Lett. **95**, 200801 (2005).

- [82] H. Frey, S. Witt, K. Felderer, and R. Guckenberger, Phys. Rev. Lett. **93**, 200801 (2004).
- [83] S. Kühn and V. Sandoghdar (2007), in preparation.
- [84] J.-C. Weeber, C. Girard, J. R. Krenn, A. Dereux, and J.-P. Goudonnet, J. Appl. Phys. **86**, 2576 (1999).
- [85] P. Anger, P. Bharadwaj, and L. Novotny, Phys. Rev. Lett. **96**, 113002 (2006).
- [86] T. Christ, F. Kulzer, P. Bordat, and T. Basche, Ang. Chem. Int. Ed. **40**, 4192 (2001).
- [87] A. Renn, J. Seelig, and V. Sandoghdar, Mol. Phys. **104**, 409 (2006).
- [88] P. Anger, P. Bharadwaj, and L. Novotny, Phys. Rev. Lett. **96**, 113002 (2006).
- [89] J. Alda, J. Rico-Garcia, J. Lopez-Alonso, and G. Boreman, Egypt. J. Solids **28**, 1 (2005).
- [90] K. Crozier, A. Sundaramurthy, G. Kino, and C. Quate, J. Appl. Phys. **94**, 4632 (2003).
- [91] J. Greffet, Science **308**, 1561 (2005).
- [92] K. Joulain, R. Carminati, J.-P. Mulet, and J.-J. Greffet, Phys. Rev. B **68**, 245405 (2003).
- [93] M. Käll, H. Xu, and P. Johansson, J. Raman Spect. **36**, 510 (2005).
- [94] N. Calander and M. Willander, J. Appl. Phys. **92**, 4878 (2002).
- [95] J. Li, A. Salandrino, and N. Engheta (2007).
- [96] H. F. Hofmann, T. Kosako, and Y. Kadoya, New J. Phys. **9**, 217 (2007).
- [97] H. Gersen, M. Garcia-Parajo, L. Novotny, J. Veerman, L. Kuipers, and N. van Hulst, Phys. Rev. Lett. **85**, 5312 (2000).
- [98] M. Lieb, J. Zavislan, and L. Novotny, J. Opt. Soc. Am. B **21**, 1210 (2004).
- [99] E. Hellen and D. Axelrod, J. Opt. Soc. Am. B **4**, 337 (1987).
- [100] H. Arnoldus, J. Opt. Soc. Am. A **22**, 190 (2004).
- [101] S. Quabis, R. Dorn, M. Eberler, O. Glöckl, and G. Leuchs, Opt. Comm. **179**, 1 (2000).
- [102] F. Kaminski, V. Sandoghdar, and M. Agio, J. Computational and Theoretical Nanoscience **4**, 635 (2007).
- [103] L. Rogobete, F. Kaminski, A. Mohammadi, M. Agio, and V. Sandoghdar (2007), in preparation.
- [104] P. K. Aravind, A. Nitzan, and H. Metiu, Surf. Science **110**, 189 (1981).
- [105] J. Aizpurua, G. W. Bryant, L. J. Richter, F. J. G. de Abajo, B. K. Kelley, and T. Mallouk, Phys. Rev. B **71**, 235420 (2005).
- [106] Note that field  $\mathbf{E}_{\text{inc}}$  now originates from the emitting molecule
- [107] PMMA: polymethyl methacrylate
- [108] DiI: dioctadecylindocarbocyanine